University of Plymouth

PEARL **https://pearl.plymouth.ac.uk**

Faculty of Science and Engineering School of Engineering, Computing and Mathematics

2023-03

Developed graphene/Si Schottky junction solar cells based on the top-window structure

Busaidi, HA

http://hdl.handle.net/10026.1/20343

10.1016/j.cartre.2023.100247
Carbon Trends
Elsevier BV

All content in PEARL is protected by copyright law. Author manuscripts are made available in accordance with publisher policies. Please cite only the published version using the details provided on the item record or document. In the absence of an open licence (e.g. Creative Commons), permissions for further reuse of content should be sought from the publisher or author.

Carbon Trends 10 (2023) 100247

Contents lists available at ScienceDirect

Carbon Trends

journal homepage: www.elsevier.com/locate/cartre

Developed graphene/Si Schottky junction solar cells based on the top-window structure

Hilal Al Busaidi[a,*], Ahmed Suhail[a,b,*], David Jenkins[a], Genhua Pan[a]

[a] Wolfson Nanomaterials & Devices Laboratory, School of Engineering, Computing and Mathematics, University of Plymouth, Devon PL4 8AA, United Kingdom
[b] Department of Physics, College of Science, University of Mosul, Mosul, Iraq

ARTICLE INFO

Keywords:
Graphene/Si Schottky junction solar cell
A sputtering process
Top-window structure
Ideal J-V curves
Stable doped devices

ABSTRACT

Chemical Vapor Deposition (CVD)-graphene has potentially been integrated with silicon (Si) substrates for developing graphene/n-Si Schottky junction solar cells prepared with the top window structure. However, there are drawbacks to prepared devices such as complex silicon dioxide (SiO_2)-etching steps, low fill factors and stability of doped devices. In this work, SiO_2 patterns are simply formed using a sputtering process rather than the previous complex method. Additionally, the fill factor for prepared devices is developed by using transferred residue-free multi-graphene layers. The usage of 3 graphene layers improves the power conversion efficiency (*PCE*) to 7.1%. A recorded PCE of around 17% with a fill factor of 74% is achieved by the HNO_3 dopant. To overcome the issue of stability, Poly(methyl methacrylate) as an encapsulated layer is introduced. Hence, the doped devices show great stability for storage in air for 2 weeks, and devices recovered about 95% of their efficiency. This work shows that the developed fabrication process is suitable to develop simple, low cost, stable and efficient graphene/Si Schottky solar cells.

1. Introduction

Due to the attractive characteristics of graphene, it has been used to prepare graphene devices such as solar cells [1]. Several structures have been developed to develop graphene/n-silicon (Si) Schottky junction solar cells [2–4]. One of those structures is the top-window structure [2], which has been widely reported for the fabrication process. In this structure, Si samples are thermally oxidized SiO_2 layer and followed by selective corrosion of silicon dioxide (SiO_2) through the complex wet-etching process using a buffered oxide etch (BOE), leading to obtaining a patterned square window for the Schottky junction [5]. However, the complex wet-etching process for that essentially increases the cost and complexity of preparing devices. To form the contact of graphene, a SiO_2 is coated with gold (Au) using the thermal evaporation method [3]. However, this method is costly, and the manufacturing process of that will be more expensive. The efficiency of devices has been improved by using several approaches. For example, chemical doping was applied to increase the built in potential and the Schottky barrier height. This improved the efficiency of doped-graphene/Si solar cells to around 10% [3,6,7]. By using the optimal oxide thickness for Si substrates and antireflection techniques (ARC), the performance of doped devices has further been improved to about 15% [8]. However, the performance of devices reduces with time. It has also been reported that doped devices will have non-ideal (s-shape) in Current-Voltage Characteristic (*J-V*) curves with time [2,4,9–18]. These disadvantages are due to the evaporation of dopants with time [17,19]. This shows that this approach is not the right for achieving efficient and stable devices. In addition, the Poly(methyl methacrylate) (PMMA) residue also causes the s-shape and results in poor performance of devices prepared using monolayer graphene [4,18,20,21]. In our previous work, it also confirms the PMMA residue traps electrons, and the DUV procedure was involved to eliminate the residue of graphene transferred with a PMMA concentration of 10 mg/ml [4]. This also shows that transferring multi-graphene layers (MGLs), which form the junction, will cause serious effects on graphene/n-Si devices since the amount of residue will be higher in this case. Based on the above discussion, it can be noticed that graphene/n-Si Schottky junction solar cells are still in need of extra development to be compared with stable, efficient and commercial silicon solar cells.

Herein, we develop and simplify the fabrication process of devices. MGLs are also successfully introduced within the preparation process to additional advance the performance of devices after eliminating the residue of PMMA by using the combination of DUV treatment along with forming gas. The doping process using HNO_3 is efficiently engaged to achieve efficient and stable devices under air conditions.

* Corresponding authors.
E-mail addresses: hilal.albusaidi@plymouth.ac.uk (H.A. Busaidi), ahmed.198381@uomosul.edu.iq (A. Suhail).

https://doi.org/10.1016/j.cartre.2023.100247
Received 1 October 2022; Received in revised form 12 December 2022; Accepted 2 January 2023
2667-0569/Crown Copyright © 2023 Published by Elsevier Ltd. This is an open access article under the CC BY-NC-ND license (http://creativecommons.org/licenses/by-nc-nd/4.0/)

2. Materials and methods

2.1. Device fabrication

Si samples were firstly occupied in the KOH solution with a concentration of 25 wt% for 2 min to eliminate the saw damage. After that, an RCA procedure was introduced to for getting rid of contaminations of the metal ion. Then, Si samples were occupied in a 2% HF solution for 30 s to eliminate the native oxide. To achieve the passivation process, samples were left under the ambient air for 2 h [8,22,23]. By using a sputtering technique at 10^{-7} Torr along with conventional lithography, substrates were coated with SiO_2/Cr/Au layers, those layers will form the required window as shown in Figs. S1b, S1c and S1d. To form the Schottky junction, a 3.3×3.3 mm^2 area of monolayer graphene supported with a PMMA layer with a concentration of 46 mg/ml concentration was transferred using a conventional wet-transfer process onto the window as presented in Fig. S1e. To minimalize the residue of PMMA obtained from the wet transfer process, DUV treatment was employed for 10 min before removing the PMMA layer. Then, PMMA layers were removed by acetone and followed by annealing in forming gas for 3 h to essential ensure less amount of PMMA residue. To form cathodes for devices, substrates were sputtered with Cr/Au layers as shown in Fig. S1h. To enhance the p doping level in graphene, devices were exposed to 65%HNO_3 for 90 s. The doped devices were coated with a PMMA layer to avoid the evaporation of HNO_3 with time.

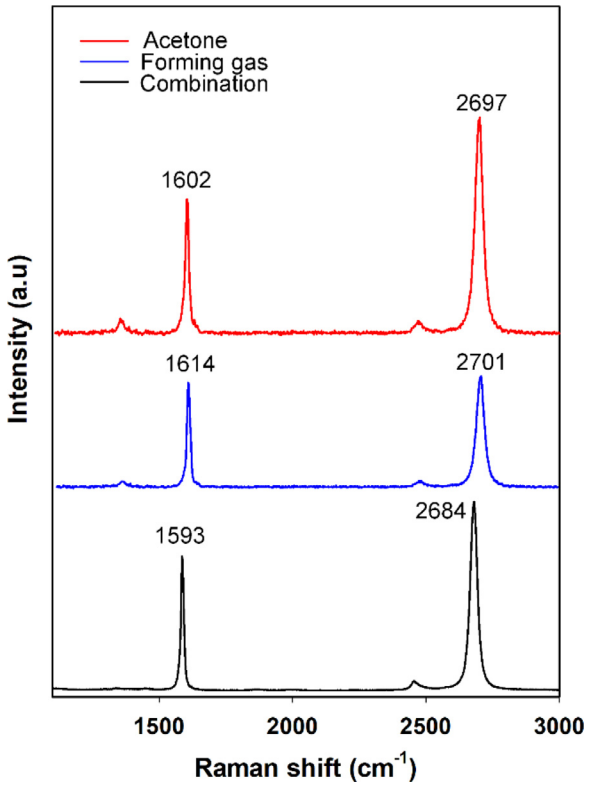

Fig. 1. Raman spectra of transferred graphene onto SiO_2/Si samples treated with acetone, forming gas and combination processes.

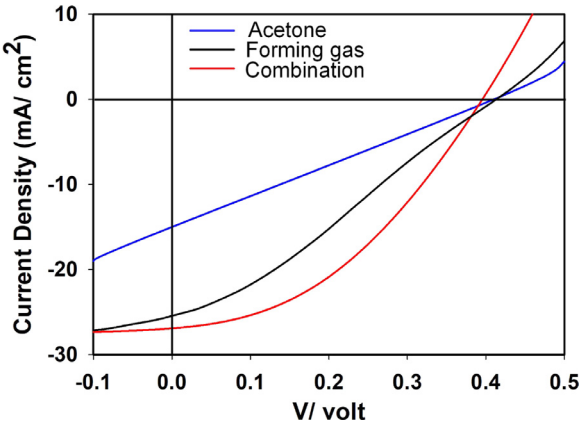

Fig. 2. *J-V* characteristics of graphene/Si Schottky solar cells that are processed with and without the combination process.

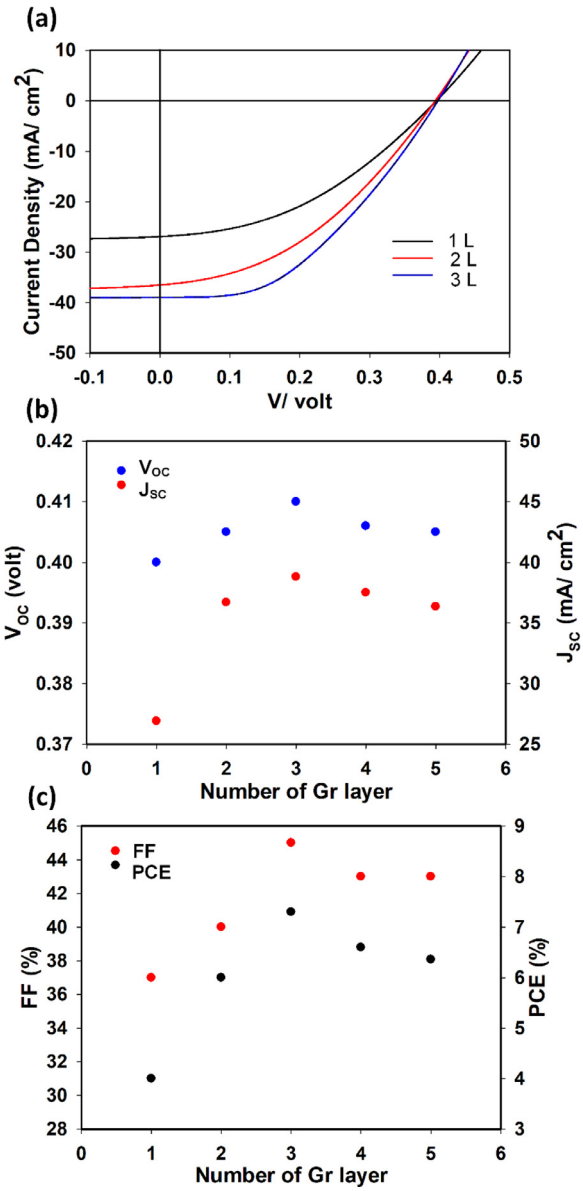

Fig. 3. (a) *J-V* curves of graphene/n-Si Schottky junction solar cells prepared with a different number of graphene layers. (b) and (c) Developments of photovoltaic factors of devices processed with a different number of graphene layers.

2.2. Device characterization

To examine the quality of graphene samples that were transferred by using the combination process, Raman tool, X-ray photoelectron spectroscopy (XPS) and Scanning Electron Microscope (SEM) were conducted. The photovoltaic characteristics of prepared devices were mea-

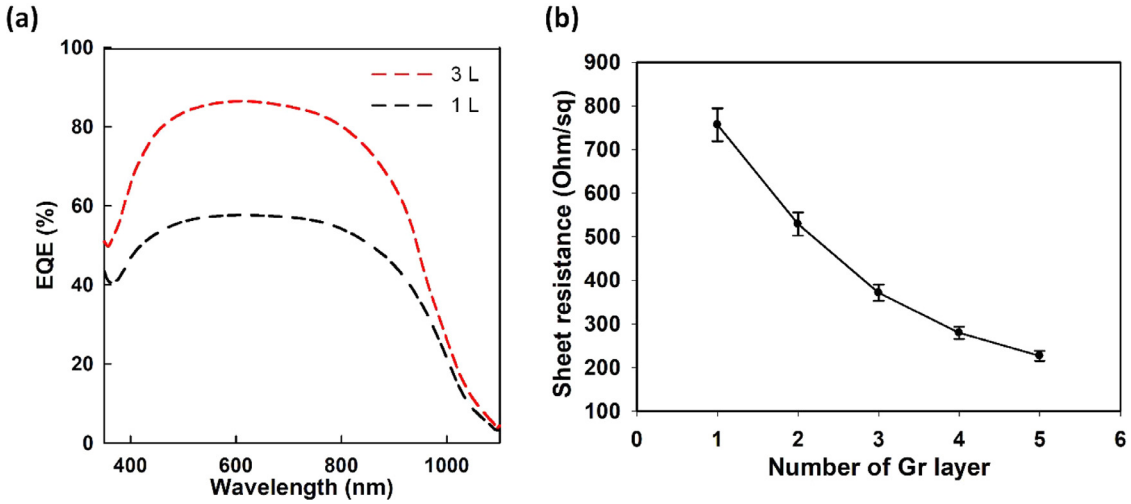

Fig. 4. (a) External quantum efficiency (EQE) curves of graphene/n-Si Schottky junction solar cells manufactured with a single and 3 graphene layers. (b) Developed sheet resistivity as a function of multi-graphene layers, showing decreases in the sheet resistance with the number of layers.

sured by using a key-sight B1500A Analyser under conditions of AM1.5 and the 100 mW/cm^2 illumination intensity after calibrating the equipment. The PVE300 system was conducted to obtain the external quantum efficiency (EQE) of the prepared devices.

3. Results and discussion

A sputtering technique with conventional lithography was introduced to simplify the manufacture of the top-window structure of graphene/Si solar cells as presented in Fig. S1. To ensure efficiently reduce the PMMA residue, the combination process including DUV and forming gas was developed for transferring residue-free graphene samples in this work. The combination process was used since forming gas alone for minimizing the PMMA residue is not efficient [4]. Raman and XPS techniques were conducted to examine the quality and PMMA residue left on transferred graphene samples. Fig. 1 shows Raman data of graphene samples, and it can be detected that the spectrum of transferred graphene that was treated with acetone (red line) verifying the monolayer nature of graphene samples. It is also displayed that the 2D and G bands are at 2697 and 1602 cm^{-1}, respectively. The intensity ratio (I_{2D}/I_G) is around 1.7. It can also be realized that there is a slight D peak at 1356 cm^{-1}, which is indicating to the defects [24–26]. After annealing samples in forming gas, it is clear there is a shift in the spectrum (blue line) in comparison with the spectrum of samples processed with acetone, showing the intensity ratio of 1. After applying the combination process, a red shift in the spectrum of graphene is obtained, indicating that the PMMA residue is reduced. In addition, the intensity ratio increased after using the combination process, showing the higher quality that was annealed in forming gas. The reduction of PMMA residue has also been confirmed by the XPS tool as shown in Fig. S4. As presented in this figure, there is a clear enhancement in the sp^2 component (red curve) that belongs to graphene. in the residue of PMMA unlike other components related to the residue after introducing the combination process. Fig. 2 illustrates the current density-voltage (*J-V*) curves of solar cells that were processed with and without the combination process, where these samples were prepared with optimum 250 nm SiO_2. For the processed device with acetone, the fill factor (*FF*), power conversion efficiency (*PCE*), open circuit voltage (V_{OC}) and short-circuit current density (J_{SC}) are 23%, 1.4%, 0.41 V and 14.7 mA/cm^2, respectively. For the processed device with forming gas treatment, the V_{OC}, J_{SC}, *FF* and *PCE* were 25 mA/cm^2, 0.413 V, 27% and 2.9%, respectively. The samples processed with the combination process show a remarkable development compared with other samples. In this case, the J_{SC}, V_{OC}, *FF* and *PCE* were 26.9 mA/cm^2, 0.4 V, 37% and 4%, respectively. This development is achieved due to minimalizing the residue of PMMA. It can clearly be observed in Fig. 2, there is an ideal *J-V* curve of samples treated with the combination technique in comparison with other curves for samples that were processed with forming gas and acetone. This also shows the residue causes the s shape and reduces the performance of devices. In addition, it is confirmed that forming gas (90% Ar/10% H_2) alone is not enough to efficiently eliminate the residue, which is also in good agreement with reported works [24–27]. It has also been reported that the residue reasons for the recombination process of carriers at the interface of graphene/Si devices, which leads to the s-shape in the *J-V* curve [4,21]. After minimalizing the residue of PMMA by the combination procedure and optimizing the SiO_2 thickness, multi-graphene layers (MGL) were employed to extra advance the fill factor. In this circumstance, the combination procedure was applied after transferring each graphene layer to effectively ensure the PMMA residue-free graphene surface. Figs. 3a and S5 demonstrate the *J-V* curves of MGL/Si devices. As observed, devices manufactured with 3 graphene layers express a significant development compared with that of other devices. The photovoltaic parameters of this device increased to 38.8 mA/cm^2, 0.415 V, 45% and 7.3% respectively. This signs that the *PCE* and *FF* developed by around 85% and 30%, respectively. To the best of our thought, the *PCE* of 7.2% is a new record for devices manufactured without doping, texturing process and anti-reflection coating reported to date [3,4,8,28,29]. This indicates that removing the PMMA residue is essential to improve the performance of MGL/Si Schottky junction solar cells. Fig. 3b and 3c show the developed photovoltaic parameters for devices prepared with MGL. As observed, the parameters for samples prepared with more than 3 graphene layers show a marginal reduction, which indicates that the optical transparency of more than 3 graphene layers is reduced [5].

Table 1
Comparison study for the high performance of doped graphene/Si Schottky junction solar cells that have been reported.

Applied techniques	*PCE (%)*	References
Top grid with doping	5.9	3
Top grid with Directly grown graphene and doping	9.18	7
Back contact with texturing process and doping	14.1	4
Top window with Interfacial Oxide, doping and ARC	15.6	22
Top window with MGL, doping and ARC	17	This work

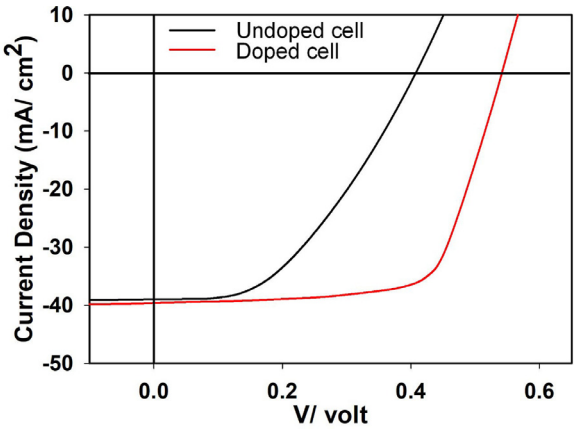

Fig. 5. *J-V* characteristics for graphene/Si Schottky junction solar cells prepared with 3 graphene layers before and after the doping process.

This means that 3 graphene layers are optimum for developing the efficiency of devices. The EQE results of devices also verify that there is a remarkable improvement in the performance of devices after introducing 3 graphene layers, compared with that of devices processed with a single graphene layer as shown in Fig. 4a. This improvement is in an excellent agreement with those obtained from the *J-V* curves. Fig.4b represents the sheet resistivity values for multi-graphene layers. It can be recognized that there is minimizing of the sheet resistivity values with increasing the number of graphene layers. It can also be realized that the sheet resistivity of 3 graphene layers was reduced to around half of that of one transferred-graphene layer, which showed the highest performance of prepared devices. For additional development, devices were doped by HNO_3. The doping process in this case was applied for 90 s. Fig. 5 displays the *J-V* curve of the treated device with HNO_3. It can be noticed that the *J-V* curve for doped devices expresses an important enhancement in performance compared with that of un-doped devices. In this case, the V_{OC} and J_{SC} developed to 0.53 V and 39.5 mA/cm^2, respectively after doping. In addition, the *FF* and *PCE* increased to 69% and 14.3%, respectively. The developed performance of doped devices indicates the conductivity of transferred graphene enhanced after doping [21,30]. Although the effective *PCE* was obtained after the doping process, the performance of doped devices with HNO_3 reduces with time since this dopant will be evaporated [17,19]. Hence, prepared devices were coated with a PMMA layer as shown in Fig. 6a. to ensure the efficient stability of the doped devices. This will prevent the evaporation of HNO_3 during this time. There is another advantage of the usage of the PMMA layer, which is for reducing the reflection of light. Fig. 6b shows *J-V* curves of coated devices with and without a layer of PMMA after the doping process. The obtained photovoltaic parameters in the case of coated samples were 42.8 mA/cm^2, 0.53 V, 74% and 16.8%, respectively. It can be noticed from this figure that J_{SC} increased from 39.5 to 42.8 mA/cm^2 after coating, compared with that of the uncoated sample. This indicates that the reflection from Si samples is reduced by the PMMA layer as shown in Fig. S6. This results in an improvement in the *PCE* and *FF*. It can also be recognized that the obtained *PCE* of 16.8 is the highest efficiency reported so far based on the best of our understanding as displayed in Table 1 [3,4,7,8,28,29,31–37]. After that, samples coated with and without PMMA layers were left in the air for 2 weeks. Then, the performance of these devices was measured after 2 weeks. The *PCE* of the coated devices was 15.9%, which indicates that the device retained 95% of its performance. In contrast, the *PCE* of un-coated devices was 10%, which indicates that the device retained 70% of its initial performance after storing. This also shows that doped devices displayed the highest stability compared with doped devices with HNO_3 in the reported works [4,17]. Hence, introducing the layer of PMMA plays a central role in obtaining stable and efficient doped graphene/Si Schottky junction solar cells.

4. Conclusions

In this work, a sputtering technique was engaged to simplify and reduce the cost of the fabrication procedure of graphene/n-Si Schottky junction solar cells. This technique along with conventional lithography also avoided the complex etching process of SiO_2. In addition, the fill factor was efficiently developed by introducing multi-graphene layers rather than monolayer graphene to obtain the Schottky junction for devices after minimizing the PMMA residue, leading to an enhancement in efficiency. The performance of devices further increased after including the doping process by HNO_3, resulting in a development in the PCE of 14.3%. The doped devices also displayed excellent performance with a *PCE* of 16.8% and stability for 2 weeks after introducing an encapsulated PMMA layer.

Declaration of Competing Interest

The authors declare that they have no known competing financial interests or personal relationships that could have appeared to influence the work reported in this paper.

Data Availability

The data that has been used is confidential.

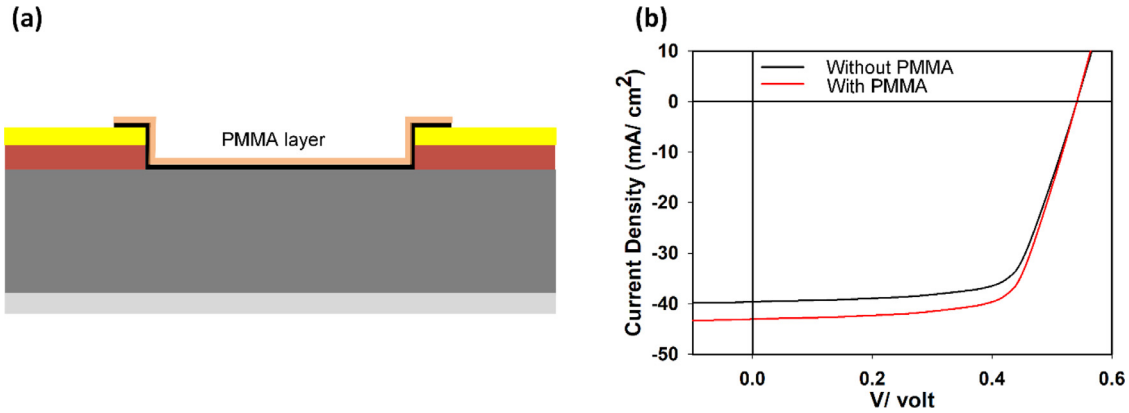

Fig. 6. (a) Schematic of MGL/Si Schottky junction solar cell coated with PMMA layer. (b) *J-V* curves for MGL/Si Schottky junction solar cells coated without and with PMMA layer.

Acknowledgment

We acknowledge the financial support from The Higher Committee for Education Development in Oman.

Supplementary materials

Supplementary material associated with this article can be found, in the online version, at doi:10.1016/j.cartre.2023.100247.

References

[1] K.S. Novoselov, et al., A roadmap for graphene, Nature 490 (7419) (2012) 192–200.
[2] X. Li, et al., Graphene-on-silicon Schottky junction solar cells, Adv. Mater. 22 (25) (2010) 2743–2748.
[3] Y. Wang, et al., Top-grid monolayer graphene/Si Schottkey solar cell, J. Solid State Chem. 224 (2015) 102–106.
[4] A. Suhail, et al., Improved efficiency of graphene/Si Schottky junction solar cell based on back contact structure and DUV treatment, Carbon 129 (2018) 520–526 N Y.
[5] B.S. Wu, et al., Hybrid multi-layer graphene/Si Schottky junction solar cells, in: Proceedings of the IEEE 39th Photovoltaic Specialists Conference (PVSC), IEEE, 2013.
[6] X. Miao, et al., High efficiency graphene solar cells by chemical doping, Nano Lett. 12 (6) (2012) 2745–2750.
[7] M.A. Rehman, et al., Thickness-dependent efficiency of directly grown graphene based solar cells, Carbon 148 (2019) 187–195 N Y.
[8] Y. Song, et al., Role of interfacial oxide in high-efficiency graphene–silicon Schottky barrier solar cells, Nano Lett. 15 (3) (2015) 2104–2110.
[9] X. An, F. Liu, S. Kar, Optimizing performance parameters of graphene–silicon and thin transparent graphite–silicon heterojunction solar cells, Carbon 57 (2013) 329–337 N Y.
[10] E. Shi, et al., Colloidal antireflection coating improves graphene–silicon solar cells, Nano Lett. 13 (4) (2013) 1776–1781.
[11] Y. Shi, et al., Work function engineering of graphene electrode via chemical doping, ACS Nano 4 (5) (2010) 2689–2694.
[12] P. Wadhwa, et al., Electronic junction control in a nanotube-semiconductor Schottky junction solar cell, Nano Lett. 10 (12) (2010) 5001–5005.
[13] X. An, et al., Tunable graphene–silicon heterojunctions for ultrasensitive photodetection, Nano Lett. 13 (3) (2013) 909–916.
[14] P. Wadhwa, et al., Electrolyte-induced inversion layer Schottky junction solar cells, Nano Lett. 11 (6) (2011) 2419–2423.
[15] W. Regan, et al., Screening-engineered field-effect solar cells, Nano Lett. 12 (8) (2012) 4300–4304.
[16] X. Li, et al., Anomalous behaviors of graphene transparent conductors in graphene–silicon heterojunction solar cells, Adv. Energy Mater. 3 (8) (2013) 1029–1034.
[17] T. Cui, et al., Enhanced efficiency of graphene/silicon heterojunction solar cells by molecular doping, J. Mater. Chem. A 1 (18) (2013) 5736–5740.
[18] A.M. Suhail, et al., Developed performance of rGO/p-Si Schottky junction solar cells, Carbon Trends 9 (2022) 100205.
[19] E. Singh, H.S. Nalwa, Stability of graphene-based heterojunction solar cells, RSC Adv. 5 (90) (2015) 73575–73600.
[20] C.J. An, et al., Ultraclean transfer of CVD-grown graphene and its application to flexible organic photovoltaic cells, J. Mater. Chem. A 2 (48) (2014) 20474–20480.
[21] A. Suhail, et al., Reduction of polymer residue on wet–transferred cvd graphene surface by deep UV exposure, Appl. Phys. Lett. 110 (18) (2017) 183103.
[22] A.G. Aberle, Surface passivation of crystalline silicon solar cells: a review, Prog. Photovolt. Res. Appl. 8 (5) (2000) 473–487.
[23] B.S. Wu, L. Yi Chun, et al., Hybrid multi-layer graphene/Si Schottky junction solar cells, in: Proceedings of the IEEE 39th Photovoltaic Specialists Conference (PVSC), IEEE, 2013.
[24] W. Choi, et al., Effect of annealing in Ar/H 2 environment on chemical vapor deposition-grown graphene transferred with poly (methyl methacrylate), IEEE Trans. Nanotechnol. 14 (1) (2015) 70–74.
[25] Z.H. Ni, et al., Tunable stress and controlled thickness modification in graphene by annealing, ACS Nano 2 (5) (2008) 1033–1039.
[26] Y.C. Lin, et al., Graphene annealing: how clean can it be? Nano Lett. 12 (1) (2011) 414–419.
[27] A. Suhail, et al., Effective chemical treatment for high efficiency graphene/si schottky junction solar cells with a graphene back-contact structure, Adv. Mater. Lett. 8 (10) (2017) 977–982.
[28] L. Yang, et al., Interface engineering for efficient and stable chemical-doping-free graphene-on-silicon solar cells by introducing a graphene oxide interlayer, J. Mater. Chem. A 2 (40) (2014) 16877–16883.
[29] S.H. Kim, et al., Performance optimization in gate-tunable Schottky junction solar cells with a light transparent and electric-field permeable graphene mesh on n-Si, J. Mater. Chem. C 5 (12) (2017) 3183–3187.
[30] S. Tongay, et al., Stable hole doping of graphene for low electrical resistance and high optical transparency, Nanotechnology 22 (42) (2011) 425701.
[31] K. Huang, et al., Progress of graphene–silicon heterojunction photovoltaic devices, Adv. Mater. Interfaces 5 (24) (2018) 1801520.
[32] D.H. Shin, et al., Remarkable enhancement of stability in high-efficiency Si-quantum-dot heterojunction solar cells by employing bis (trifluoromethanesulfonyl)-amide as a dopant for graphene transparent conductive electrodes, J. Alloys Compd. 773 (2019) 913–918.
[33] M.J. Im, et al., Sandwich-doping for a large schottky barrier and long-term stability in graphene/silicon schottky junction solar cells, ACS Omega 6 (5) (2021) 3973–3979.
[34] J.H. Kim, H.G. Kim, L.K. Kwac, High-efficient Schottky-junction silicon solar cell using silver nanowires covering nitrogen-doped amorphous carbon, Curr. Appl. Phys. 26 (2021) 1–8.
[35] M.A. Rehman, et al., Development of directly grown-graphene–silicon Schottky barrier solar cell using co-doping technique, Int. J. Energy Res. (2022).
[36] T. Chen, et al., Antireflection improvement and junction quality optimization of Si/PEDOT: PSS solar cell with the introduction of dopamine@ graphene, Energies 13 (22) (2020) 5986.
[37] C. Li, et al., Performance improvement of graphene/silicon solar cells via inverted pyramid texturation array, Silicon (2022) 1–9.